

LASER SINTERING OF PA12/PA4,6 POLYMER COMPOSITES

D. Strobbe*, P. Van Puyvelde†, J.-P. Kruth*, B. Van Hooreweder*,

* KU Leuven, Department of Mechanical Engineering, Belgium

† KU Leuven, Department of Chemical Engineering, Belgium

Abstract

This work investigates the laser sintering (LS) processing of polyamide-12/polyamide-4,6 composites and the performance of resulting parts. The coalescence and consolidation of the PA12/PA4,6 powder mixture are characterized. This demonstrates that at the LS processing window for PA12 (grade PA2200), the powder mixture exhibits bimodal melting behavior. In this behavior PA2200 melts during LS processing but PA4,6 remains solid. After laser sintering of the materials, the microstructure and the mechanical properties of the resulting parts are characterized. This illustrates that the PA2200 coalesces well and PA4,6 remains as a secondary phase during the LS processing. Further developments to improve the powder size and morphology in order to obtain better relative density of the parts are necessary. The investigated processing approach opens up new perspectives for LS of advanced engineering thermoplastics.

Keywords: Laser Sintering, polyamides

Introduction

Laser Sintering (LS) is a powder bed fusion Additive Manufacturing (AM) technique for thermoplastic polymers. Virtually every thermoplastic polymer is suited for LS, however the commercial materials are mainly limited to polyamide-12 and -11 and thermoplastic polyurethanes [4]. With the expansion of AM techniques from prototyping towards production of end-use parts, there is a pull for additively manufactured products with a broader range of material properties. The specific process characteristics of Laser Sintering imply some limitations to the polymers that can be processed: (i) the material needs to be available as a powder, with sufficient deposition quality [5]. (ii) The temperature interval between the onset of crystallization and onset of melting, termed *subcooling region* or *thermal processing window*, should be large enough in order to avoid part crystallization and shrinkage because of temperature fluctuations during production [4]. (iii) The melt viscosity should be low enough, to obtain good coalescence and no residual porosity in the fused regions [6]. (iv) The material may not degrade at the temperatures reached locally by the laser heating [7,8].

Previous work already investigated the LS behavior of polyamide-12 blended with polyamide-6 [2], HDPE [3], and PP [1]. In these works, both materials melt and form a blended microstructure with high residual porosity.

The approach of the current investigation is to make use of a mixture of two thermoplastic polymers. One thermoplastic having a significantly lower melting range than the second. This is to achieve a bimodal melting behavior. The introduction of a second, higher melting thermoplastic, is expected to already alter material properties. Additionally, this approach can overcome some of the described limitations. Only the thermal processing window and melt viscosity of the lower melting thermoplastic should be large enough, since this is the matrix phase that will consolidate

the part. Thermal shrinkage will be reduced, because less material will go through a phase transition during the process.

In this case the commercial LS standard polyamide-12 (PA2200) powder is used as a melting phase. This enables production with standard LS parameter sets. The polyamide-4,6 (PA4,6) material is selected as reinforcing phase because of its higher melting point. In this way it is expected not to melt during LS processing and to lower thermal shrinkage. Additionally, since both materials are polyamides, a good chemical compatibility is assumed. As such, the thermal processing window of PA12 can be used for processing those new materials.

Materials and methods

- **Powder materials and characterization methods**

The powders used in this investigation are polyamide-12 (PA2200, EOS) and polyamide-4,6 (PA4,6). The PA4,6 powder material is characterized by scanning electron microscopy (SEM, Philips XL30 microscope) and laser diffraction particle size distribution (PSD, Malvern Mastersizer). The thermal behavior of the materials is investigated with thermogravimetric analysis (TGA, TA Instruments Q500, N₂ atmosphere, rate 25 °C/min) and differential scanning calorimetry (DSC, TA Q2000, rate 10 °C/min). The TGA and DSC curves are analyzed with TA Universal Analysis software. The degradation temperature is determined at a weight loss of 1 wt% in the TGA. The melting and coalescence of the powder mixture is investigated using an optical microscope equipped with a hot stage.

- **Production and part characterization methods**

The powder mixtures are prepared by dry weighing the powders in the appropriate weight ratios and mechanically mixing-shaking in a Turbula mixer. Laser Sintering production was done on a DTM Sinterstation 2000 machine with a 100 W CO₂ laser with beam diameter 450 μm under N₂ atmosphere. Table 1 shows the main production parameters. The laser energy density is an engineering parameter, containing the laser power, scan speed and scan spacing, as in equation 1.

Table 1: Laser sintering production parameters

Powder bed temperature	162 °C
Laser power range	4 – 24 W
Laser scan speed range	1000 – 2000 m/s
Laser energy density range	0.025 – 0.08 J/mm ²
Layer thickness	0.1 mm
Scan spacing	0.15 mm

$$\text{Laser energy density} = \frac{\text{Laser power [W]}}{\text{scan speed [mm/s]} * \text{scan spacing [mm]}} \quad (1)$$

Single layer parts are produced and evaluated through optical microscopy (Keyence K6000). For low wt% of PA4,6 powder mixtures, multilayer parts are produced, and evaluated towards their relative density (Archimedes principle in ethanol), microstructure (optical microscopy after polishing) and tensile properties (Instron 5567, ASTM D638 Type V, 5 repetitions per data point). The viscoelastic behavior of multilayer parts are also characterized by dynamical mechanical analysis (DMA, TA Instruments Q800).

Results and discussion

- **Powder characterization**

Figure 1 shows the SEM image and the particle size distribution of the PA4,6 powder. The PA4,6 is irregular and aspherical in shape, and the average particle size is larger than that of the PA2200 powder. The PA4,6 powder is not specifically developed for LS. Further developments can improve the powder size and morphology towards smaller, more spherical particles. Increased sphericity of the particles will improve powder flow during the layer deposition and resulting packing density. Particles with a more similar particle size distribution to PA2200 will both improve powder deposition and reduce segregation between the two powders.

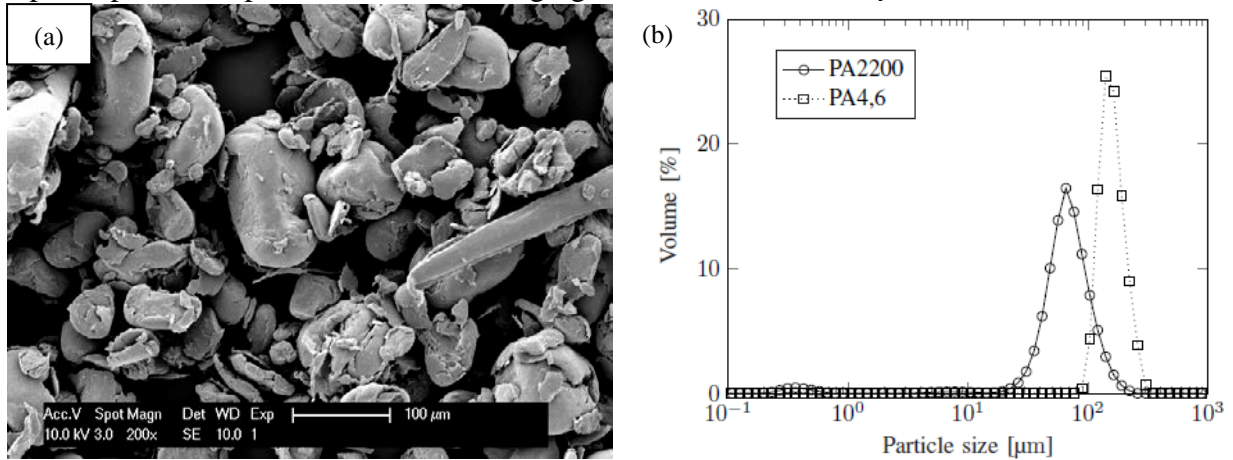


Figure 1: (a) SEM image of the PA4,6 powder and (b) Particle Size Distribution of the PA4,6 powder in comparison with PA2200

- **Thermal characterization**

During the LS process, the powder will witness two heat sources: (i) the IR preheating at powder bed temperature, and (ii) the heating by local laser exposure. The TGA and DSC profiles, together with the hot stage microscopy, provide insight in the thermal and coalescence behavior of the PA2200/PA4,6 powder mixture. Figure 2 plots the TGA and DSC profiles of the PA4,6 powder in comparison with PA2200. Table 2 shows the characteristic temperatures of the materials, as analyzed by TGA and DSC. Figure 3 provides the hotstage microscopy images of the PA2200/PA4,6 powder mixture, subject to a heating profile from 160 °C to 270 °C and subsequent cooling to 140 °C.

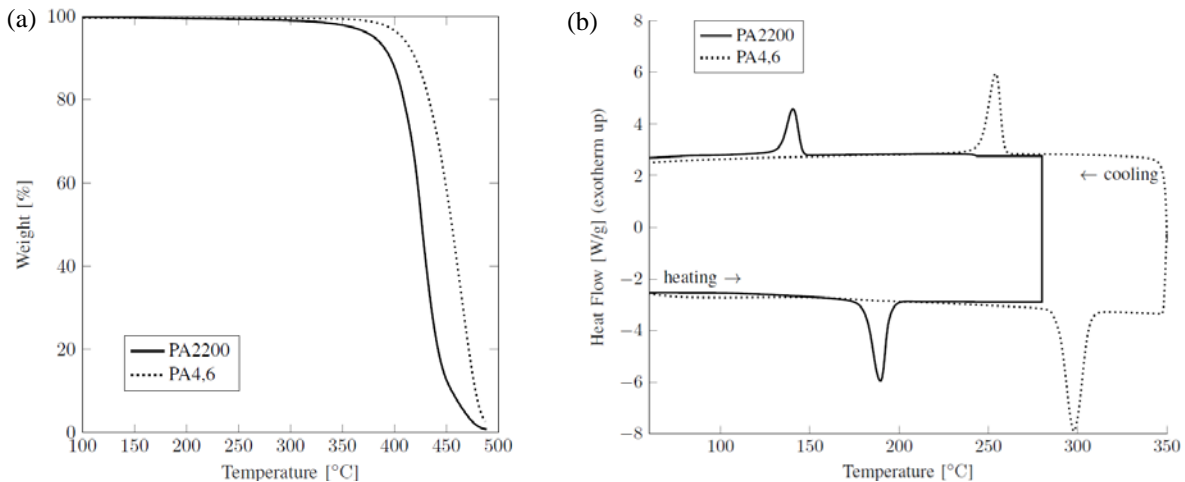


Figure 2: (a) TGA and (b) DSC curves of the powder materials

Table 2: Characteristic temperatures of the materials

	PA2200	PA4,6
Onset of melting	170.4 °C	278.7 °C
Melting temperature	189.5 °C	297.8 °C
Onset of crystallization	150.0 °C	265.9 °C
Crystallization temperature	140.5 °C	254.1 °C
Degradation temperature	299.0 °C	371.0 °C
Thermal window	150.0 – 170.4 °C	
Stable sintering region	203.5 – 299.0 °C	

The characteristic temperatures relate to the LS process as follows. The powder bed temperature will be maintained within the “thermal window” between the onset of melting and onset of crystallization of PA2200 [4]. The powder bed temperature during the tests is 162 °C. The laser exposure should lead to a temperature increase above the melting temperature of PA2200, but below its degradation temperature. This temperature interval between melting and degradation is termed the “stable sintering region” [7]. The images in Figure 3 demonstrate the coalescence behavior of the powder mixture in hot stage microscopy. When heated, the PA2200 particles melt upon heating between 180 and 190 °C, where they change from dark round particles to transparent droplets. The PA4,6 particle does not melt during the imposed temperature cycle. In the image at 200 °C the molten PA2200 droplets are flowing over the unmolten PA4,6 particle. During heating from 200 °C to 270 °C the molten PA2200 droplets gradually wet and cover the surface of the unmolten PA4,6 particle. The PA4,6 particle swells slightly at these higher temperatures of 250 °C to 270 °C, but it clearly retains its irregular shape and doesn’t form a molten droplet. Upon cooling, the PA2200 melt consolidates around the unmolten PA4,6 particle around 150 °C. This coalescence behavior is consistent with the characteristic temperatures observed in the DSC curve as shown in Table 2. The PA4,6 does not show any first order thermal transitions in temperature cycles below 270 °C. The PA2200 follows the observed melting and crystallization trajectory at the tabellized temperatures.

The images in Figure 3 confirm the “bimodal melting behavior” approach, as the PA4,6 in the powder mixture, should not melt upon laser exposure. However there are some differences between the temperature profile in hot stage microscopy and the temperature profile in laser heating. The spatial and temporal heating gradient is much higher in laser heating than in hotstage microscopy. This means that in the LS process, locally and for short times, the temperature might exceed 270 °C. This can cause thermal shrinkage, hindering layerwise production. As seen further with multilayer production this shrinkage is no problem for up to 30 wt% PA4,6. On the other side, this local and partial melting of the PA4,6 particle might also improve the adhesion of the PA2200 at the PA4,6 surface.

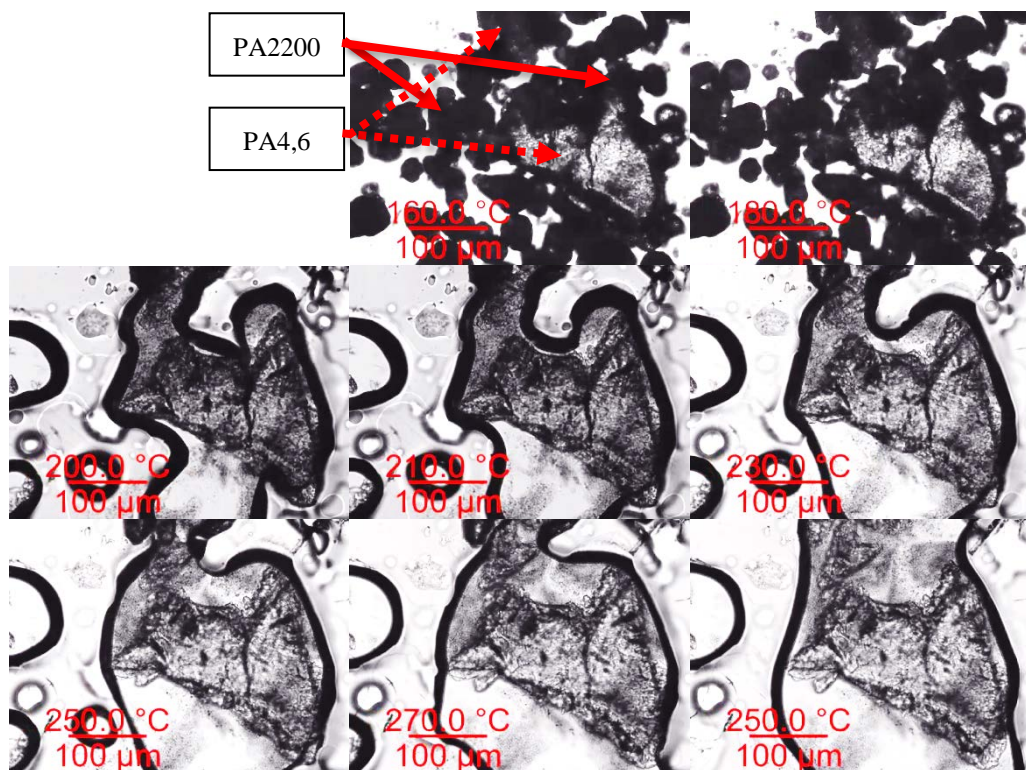




Figure 3: Hot stage optical microscopy images of a mixture of PA2200 and PA4,6, with a heating from 160 °C to 270 °C and subsequent cooling to 140 °C (left to right, top to bottom)

- **Part microstructure**

Figure 4 provides images of single layer samples of PA4,6/PA2200 powder mixtures at different wt% PA4,6. The increasing porosity in the single layers indicates that at higher wt% PA4,6, the coalescence and consolidation might be insufficient. However, the distinction has to be made between single layer samples and multilayer samples. In multilayer samples, the time available for coalescence after laser exposure is longer, because the part is kept at the powder bed temperature of 162 °C for a longer time and there is an influence of the laser exposure in the subsequent layers. The hot stage microscopy images in Figure 3 show that the PA2200 matrix material is still in the liquid form between 180 °C and 162 °C. At these temperatures the PA2200 wets the PA4,6 particle and has the time to fully cover the PA4,6 particle. Because of this longer coalescence time, consolidation in multilayer parts than in single layer parts is better for the same laser energy density. Figure 5 demonstrates the high relative density for low wt% PA4,6. Nevertheless, consolidation of the powder mixture can be insufficient locally. This especially can

pose problems for fine features in complex parts with higher PA4,6 content, where the laser exposure in subsequent layers is less.



Figure 4: Optical microscopy images of LS single layer samples at 0.053 J/mm^2 (a) 20 wt% PA4,6 (b) 60 wt% PA4,6 (c) 80 wt% PA4,6

Based on relative density measurements of the multilayer parts (as illustrated in Figure 5), a laser energy density of 0.04 J/mm^2 was found to result in optimal part density. The pores do not seem to directly appear at the interface of the PA4,6 particles. Possible mechanism that cause the increased porosity are (i) the segregation of the heavier and larger PA4,6 particles during powder deposition, (ii) changes in crystallinity of the PA2200 matrix material or (iii) lower initial packing density of the powder mixture caused by the irregular PA4,6 particle shape.

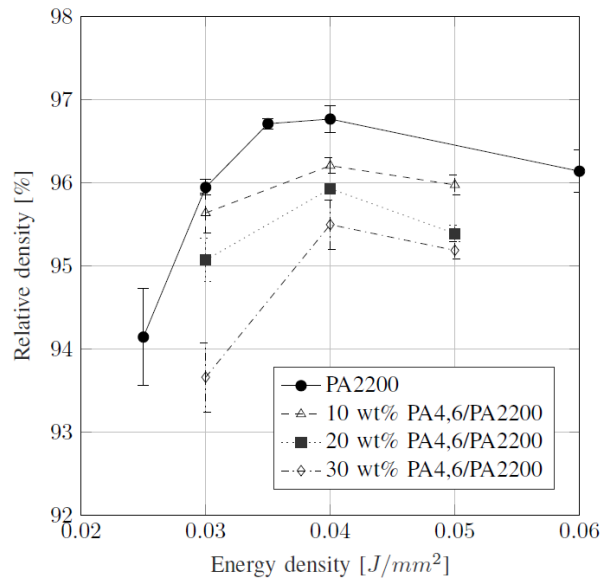


Figure 5: Relative density of multilayer parts with different wt% PA4/6 at different laser energy density.

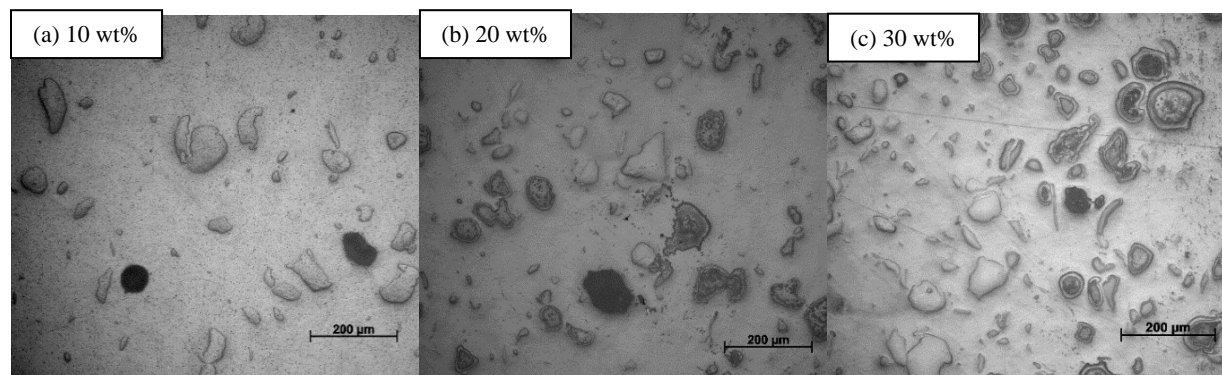


Figure 6: Optical microscopy images of LS multilayer samples at 0.04 J/mm^2 , after polishing.

- **Mechanical properties**

Figure 7 shows the tensile properties for the PA4,6/PA2200 parts in comparison with LS PA2200 properties. There is a clear decrease in tensile strength and elongation at break with increasing PA4,6 content. Next to the decrease in relative density (Figure 5), bad interfacial strength between the two material phases contribute to this decrease in mechanical properties. At the interface between the two phases, the material typically consolidates in a less ordered structure, with lower mechanical integrity. The E-modulus slightly increases with increasing PA4,6 content. Further developments should be pointed at improving the relative density and studying the interfacial adhesion between the two polymeric phases. In this way, an increase in both strength and stiffness might be achieved.

Figure 8 plots the results of the DMA analysis. There is a slight increase in storage modulus at higher temperatures. The storage modulus as observed in the DMA measurements, is correlated with the E-modulus of the material. Higher DMA storage modulus thus indicates higher E-modulus at elevated temperatures. The service temperature of a polymer material depends on the mechanical modulus at elevated temperatures, thermal degradation behavior and long term creep properties. The modulus at elevated temperatures is shown to be improved as shown the DMA in Figure 8. The degradation temperature of one of the composing materials is $72 \text{ }^\circ\text{C}$ higher as measured by TGA (Figure 2a, Table 2). Two effects contributing to service temperature have been improved. This suggest higher service temperatures can be reached by reinforcing PA2200 with PA4,6. Depending on the specific application, service temperature characterization contains more extensive mechanical testing protocols.

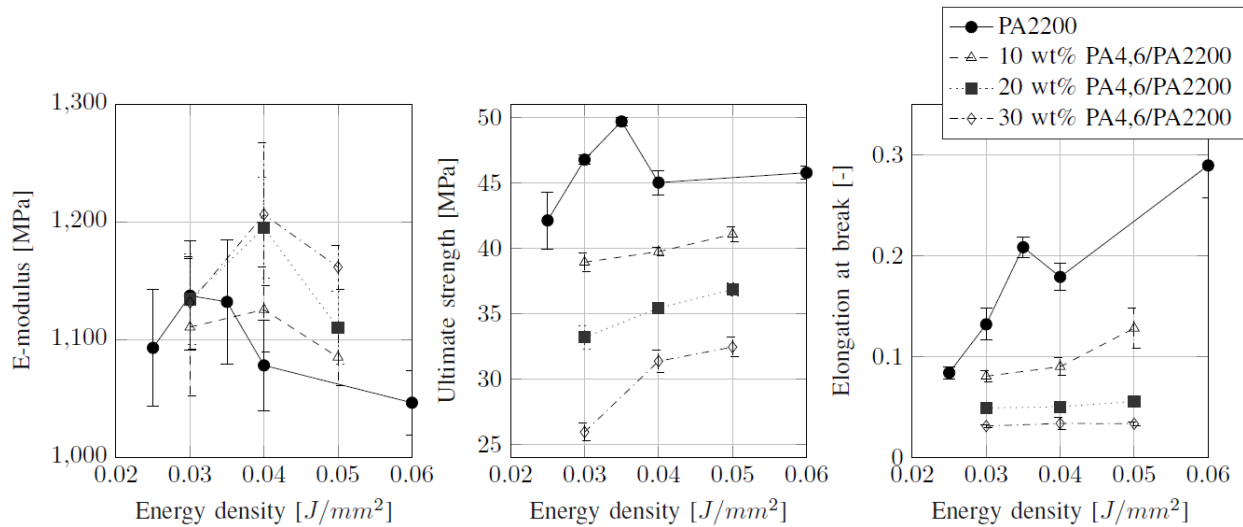


Figure 7: Tensile properties of 10 wt%, 20 wt% and 30 wt% PA4,6 samples, in comparison with pure PA2200

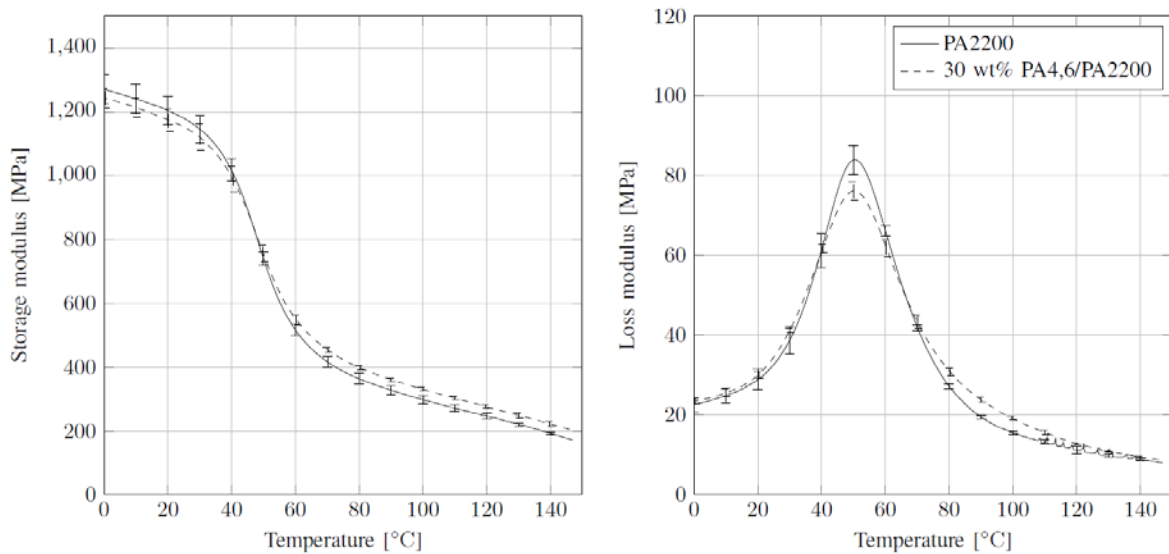


Figure 8: DMA analysis of laser sintered 30 wt% PA4,6/PA2200 and laser sintered PA2200 as a comparison.

Conclusions and future work

The investigation gives a proof-of-concept of the “bimodal melting approach” for Laser Sintering. This approach makes use of a mixture of two polymeric powders of which one coalesces during LS processing (PA2200) and the other one acts as a reinforcing phase (PA4,6). In this way plastic parts with greater diversity in mechanical and functional properties, are produced by using standard commercial process parameter sets. Parts with relative density up to 96 % are produced. For higher wt%-content of the reinforcing phase, coalescence of the PA2200 is hindered, leading to lower part density and unsatisfying mechanical properties.

Regarding this specific powder mixture, the change in powder packing density, thermal shrinkage, crystallinity, partial melting of the non-melting phase and chemical interactions between the polymers at the interface can still be analyzed more in depth. Furthermore, the local distribution

of the reinforcing powder and the pores for parts with varying dimensions will be an important point of attention for functional parts.

The approach has shown to mitigate some specific LS material requirements, such as low melt viscosity and a large thermal processing window. This allows extension to other advanced engineering thermoplastics such as PEAK and TPF. A main focus will then be the achievable resulting material properties.

Acknowledgements

The authors like to thank Strategic Initiatives Materials (SIM) Flanders for the funding, the Department of Materials Engineering of the KU Leuven for the use of their infrastructure and Mr. Lander Matthé for the conducted tests and experiments.

References

- [1] D. Drummer, K. Wudy, F. Kühnlein, and M. Drexler, "Polymer Blends for Selective Laser Sintering: Material and Process Requirements," *Phys. Procedia*, vol. 39, pp. 509–517, 2012.
- [2] G. V. Salmoria, J. L. Leite, and R. A. Paggi, "The microstructural characterization of PA6/PA12 blend specimens fabricated by selective laser sintering," *Polym. Test.*, vol. 28, no. 7, pp. 746–751, 2009.
- [3] G. V. Salmoria, J. L. Leite, C. H. Ahrens, A. Lago, and A. T. N. Pires, "Rapid manufacturing of PA/HDPE blend specimens by selective laser sintering: Microstructural characterization," *Polym. Test.*, vol. 26, no. 3, pp. 361–368, 2007.
- [4] R. D. Goodridge, C. J. Tuck, and R. J. M. Hague, "Laser sintering of polyamides and other polymers," *Prog. Mater. Sci.*, vol. 57, no. 2, pp. 229–267, 2012.
- [5] M. Van den Eynde, L. Verbelen, and P. Van Puyvelde, "Assessing polymer powder flow for the application of laser sintering," *Powder Technol.*, vol. 286, pp. 151–155, 2015.
- [6] L. Verbelen, S. Dadbakhsh, M. Van Den Eynde, J. P. Kruth, B. Goderis, and P. Van Puyvelde, "Characterization of polyamide powders for determination of laser sintering processability," *Eur. Polym. J.*, vol. 75, pp. 163–174, 2016.
- [7] G. M. Vasquez, C. E. Majewski, B. Haworth, and N. Hopkinson, "A targeted material selection process for polymers in laser sintering," *Addit. Manuf.*, vol. 1, pp. 127–138, 2014.
- [8] J. P. Kruth, G. Levy, F. Klocke, and T. H. C. Childs, "Consolidation phenomena in laser and powder-bed based layered manufacturing," *CIRP Ann. - Manuf. Technol.*, vol. 56, no. 2, pp. 730–759, 2007.